Surface Properties of Kuiper Belt Objects and Centaurs from Photometry and Polarimetry

Irina N. Belskaya
Kharkiv National University

Anny-Chantal Levasseur-Regourd
Université Pierre et Marie Curie (Paris 6)/Aéronomie

Yuriy G. Shkuratov
Kharkiv National University

Karri Muinonen
University of Helsinki

Physical properties of Kuiper belt objects (KBOs) can be assessed by studying their photometric and polarimetric phase effects close to opposition, i.e., the brightness opposition effect and the negative polarization branch. The first phase-curve observations and their promising preliminary interpretations are reviewed for KBOs and Centaurs. Despite the limited range of phase angles accessible from groundbased observations, distinct features have been discovered both in brightness and polarization. Recent results of relevant numerical and laboratory simulations of phase-angle effects are reviewed. The possibility of constraining the geometric albedos of the surfaces based on photometric and polarimetric observations is discussed.

1. INTRODUCTION

Probing the surface properties of solar system objects by photometric and polarimetric observations at different phase angles (angle between the Sun and the Earth as seen from the object) is a traditional technique in solar system remote sensing. Scattered light measured at varying illumination and observation geometries contains information about the physical properties of the topmost surface layer such as particle size, heterogeneity, complex refractive index, porosity, and surface roughness. The physical parameters define such observable parameters as the geometric albedo of the surface. The intricate inverse problem to constrain surface properties from phase-angle-resolved photometry and polarimetry is almost the only way to assess the microscopic properties of the surface from remote observations.

In the particular case of Kuiper belt objects (KBOs), the geometry of groundbased observations is limited to small phase angles, with the maximum accessible phase angle being α_{max} = arcsin (1/r), where r is the heliocentric distance in AU. For transneptunian objects (TNOs), the phase-angle range is typically less than 2°, increasing to 7°–8° for Centaurs. These distant objects are thus observable only close to the backscattering direction.

At small phase angles, two intriguing phenomena are typically observed for solid atmosphereless solar system bodies: the so-called opposition effect in brightness and the negative branch in the degree of linear polarization. The opposition effect manifests itself as a considerable nonlinear increase of surface brightness as the phase angle decreases to zero. Negative polarization is a peculiar case of partially linearly polarized scattered light where the electric field vector component parallel to the scattering plane predominates over the perpendicular component. Observations of the abovementioned opposition phenomena for various kinds of solar system bodies have a long history, whereas the understanding of their physical nature has progressed considerably only during the last two decades (for reviews, see, e.g., *Muinonen et al.,* 2002; *Shkuratov et al.,* 2004). There are several physical mechanisms that may contribute to the opposition phenomena depending on the properties of the surfaces. Both opposition phenomena are considered to have, at least partly, similar physical causes and their joint analysis can result in constraints on the physical properties of the surfaces under consideration.

At present, the observational data on the photometric and polarimetric phase effects of KBOs are still scarce for any statistical conclusions. Polarimetric observations of KBOs have just begun and many of the photometric observations are of insufficient accuracy for the derivation of firm conclusions.

In the present chapter, we focus on the study of the opposition phenomena for KBOs and Centaurs and on what constraints can be derived for the surface properties on the basis of such a study. In section 2, we review the photometric and polarimetric observations of KBOs and Centaurs, with emphasis on the phase effects. Polarimetry is here described in more detail, whereas photometry is also discussed in the

chapter by Sheppard et al. Section 3 gives a brief description of the physical mechanisms for the opposition phenomena and describes recent results of relevant numerical and laboratory simulations. In section 4, we compare the KBO observations to those of other solar system bodies and discuss which surface properties can be constrained by the observations. Finally, we outline the future prospects of the photometric and polarimetric studies.

2. OBSERVATIONS

2.1. Advances in Photometry

The first tentative derivations of the magnitude dependences on the phase angle for a few KBOs were obtained as a byproduct of the observational programs devoted to the determination of the rotational properties of KBOs. *Sheppard and Jewitt* (2002) reported phase curves of seven KBOs in the R band, with a small number (2–4) of observations within phase angles less than 2°. The authors emphasized the similarity of the phase coefficients (slopes in the phase curves) for all KBOs studied, with the mean phase coefficient being large at $\beta = 0.15$ mag/deg, suggesting comparative uniformity of the surface properties. Independently, *Schaefer and Rabinowitz* (2002) carried out numerous photometric observations for the KBO (38628) Huya and derived a comparable phase coefficient of 0.125 ± 0.009 mag/deg in the R band. They concluded that the observed magnitude variations of (38628) Huya vs. the phase angle (ranging 0.3°–2.0°) are consistent with a linear dependence. Additional phase curves were published by *Rousselot et al.* (2003, 2005a), *Boehnhardt et al.* (2004), and *Bagnulo et al.* (2006).

Magnitude dependences were also observed for a few Centaurs in a larger range of phase angles up to 7° in the R band (*Bauer et al.,* 2002, 2003; *Rousselot et al.,* 2005a; *Bagnulo et al.,* 2006) and for the Centaur (10199) Chariklo in the J band (*McBride et al.,* 1999). The phase curves were fitted according to the H, G magnitude system with G values ranging from –0.39 to 0.18 for the R band, considering them to be consistent with low-albedo surfaces (*Bauer et al.,* 2003). Note that the negative G values have no physical meaning and indicate problems with the H, G system. Generally, the phase curves obtained for Centaurs are mutually quite compatible within the uncertainties of the observations.

Belskaya et al. (2003) indicated a possible existence of a very narrow opposition surge starting at phase angles below 0.1°–0.2°. For all available observations at such extremely small phase angles, the brightness was found to be systematically higher than the brightness extrapolated from a linear phase function. The same result was obtained for the TNO (55637) 2002 UX_{25} observed at a phase angle of 0.02° by *Rousselot et al.* (2005a).

Photometric observations with an emphasis on extremely small phase angles were made by *Hicks et al.* (2005) for the TNO (20000) Varuna. They found an opposition surge of about 0.1 mag at phase angles less than 0.1°. Further observations of Varuna confirmed the pronounced opposition surge, allowing its more precise estimation (*Belskaya et al.,* 2006). The magnitude-phase dependence for Varuna is shown in Fig. 1.

Rabinowitz et al. (2007) presented a large survey dedicated to the measurements of phase curves for distant solar system objects, including 18 TNOs and 7 Centaurs. They found a wide range of phase coefficients from almost zero to 0.4 mag/deg and reported a significant wavelength dependence (from B band to I band) of the coefficients for some objects. Their conclusions are based on long-term observing campaigns with typically very few observations for an object per night. Because of the difficulties in distinguishing between the effects from rotation and varying phase angle (see discussion below), such an approach can give only rough estimates for phase coefficients.

Recalling that, in general, the phase-curve behavior near opposition is nonlinear, a linear function used for phase-curve fitting should be treated as a rough approximation for a limited phase-angle range. Thus, the values of phase coefficients depend on the phase-angle range used in the linear fitting. This is well illustrated by the phase coefficient of Varuna varying from 0.33 to 0.11 mag/deg (*Belskaya et al.,* 2006).

The values of the most accurate phase coefficients for KBOs and Centaurs are compiled in Table 1, which also gives the ranges of phase angles covered by the observations. Although the uncertainties of the phase coefficients are rather large, the observational data indicate two main features in the photometric phase curves of KBOs and Centaurs: (1) a steep linear phase dependence for most objects; (2) an opposition surge at extremely small phase angles below 0.1°.

2.1.1. Pluto. The photometric phase curve of Pluto has been observed repeatedly (*Binzel and Mulholland,* 1984; *Tholen and Tedesco,* 1994; *Buie et al.,* 1997; *Buratti et al.,* 2003). All observations show a small phase coefficient in the

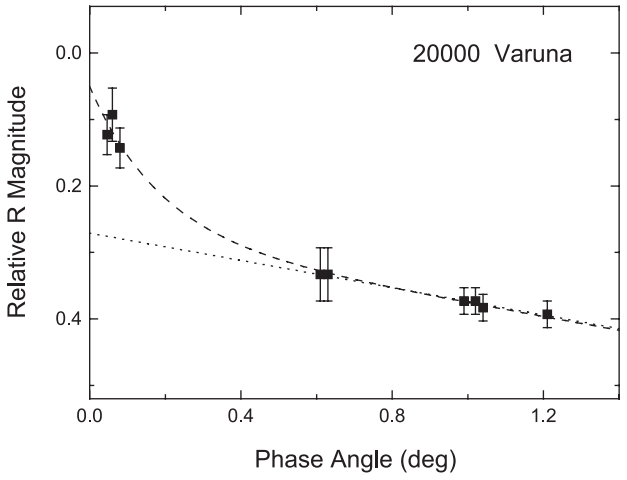

Fig. 1. Magnitude phase curve of Varuna fitted by a linear-exponential model (for details see *Belskaya et al.,* 2006).

TABLE 1. Phase coefficients measured for KBOs and Centaurs.

Object	Phase-angle range (deg)	Phase coefficient in the R band (mag/deg)	σ (mag/deg)	Reference
(2060) Chiron	1.4–4.2	0.045	0.023	*Bagnulo et al.* (2006)
(5145) Pholus	0.7–4.0	0.075	0.006	*Buie and Bus* (1992)
(10370) Hylonome	1.3–3.0	0.058	0.045	*Bauer et al.* (2003)
(20000) Varuna	0.06–1.23	0.11*	0.03	*Belskaya et al.* (2006); *Jewitt and Sheppard* (2002)
(28978) Ixion	0.25–1.34	0.20	0.04	*Boehnhardt et al.* (2004)
(29981) 1999 TD_{10}	0.77–3.5	0.12	0.06	*Rousselot et al.* (2005b)
(31824) Elatus	1.3–7.1	0.082	0.006	*Bauer et al.* (2002)
(32532) Thereus	0.2–5.6	0.072	0.004	*Rabinowitz et al.* (2007)
(38628) Huya	0.5–1.9	0.14	0.02	*Sheppard and Jewitt* (2002)
(38628) Huya	0.28–2.0	0.125	0.02	*Shaefer and Rabinowitz* (2002)
(40314) 1999 KR_{16}	0.31–1.3	0.14	0.02	*Sheppard and Jewitt* 2002
(47932) 2000 GN_{171}	0.02–2.0	0.143 (V)	0.030	*Rabinowitz et al.* (2007)
(50000) Quaoar	0.25–1.2	0.16	0.06	*Bagnulo et al.* (2006)
(50000) Quaoar	0.17–1.3	0.159 (V)	0.027	*Rabinowitz et al.* (2007)
(54598) Bienor	0.3–3.0	0.095 (V)	0.016	*Rabinowitz et al.* (2007)
(60558) Echeclus	0.1–3.9	0.18	0.02	*Bauer et al.* (2003); *Rousselot et al.* (2005a)
(90482) Orcus	0.4–1.2	0.114 (V)	0.030	*Rabinowitz et al.* (2007)
(136108) 2003 EL_{61}	0.5–1.1	0.091 (V)	0.025	*Rabinowitz et al.* (2006)
(134340) Pluto	0.6–2.0	0.029 (V)	0.001	*Buie et al.* (1997)

*Opposition surge observed at $\alpha < 0.1°$ was excluded from calculations of phase slope.

V band of 0.03–0.04 mag/deg. A nonlinear opposition surge has not been observed so far, but its existence cannot be excluded at phase angles below 0.4°, not covered by the observations. *Buratti et al.* (2003) noticed a weak wavelength dependence for the phase coefficient of Pluto ranging from 0.037 mag/deg in B to 0.032 mag/deg in R. However, most of the observations are related to the Pluto-Charon system. An attempt to constrain the individual photometric properties of these objects was made by *Buie et al.* (1997). They obtained a smaller phase coefficient for Pluto (0.029 mag/deg) and the first estimation of the phase coefficient for Charon (0.087 mag/deg) in the phase-angle range of 0.6°–2°.

Small phase coefficients, comparable to that of Pluto, were reported by *Rabinowitz et al.* (2006, 2007) for the large TNOs (136199) Eris, (136472) 2005 FY_9, and (136108) 2003 EL_{61}. They concluded that phase coefficients below 0.10 mag/deg are a salient feature for Pluto-scale TNOs with neutral colors, high albedos, and icy surfaces.

2.1.2. Uncertainties of phase coefficients. Most phase-curve observations were made with an accuracy of about 0.1 mag. Taking into account the narrow range of phase angles available, phase coefficient estimates based on such observations are not reliable. The small errors of the phase coefficients given in some papers were derived without taking into account the individual observational uncertainties pertaining to each photometric point. Using proper weights in the linear least-squares analyses, the uncertainties of the phase coefficients become considerably larger.

Another problem in deriving phase coefficients is connected to difficulties in assessing the brightness variations due to rotation. Lightcurve amplitudes were taken into account only for a few objects. The values of the phase coefficients derived by omitting the lightcurve variations should be treated with great caution. For precise derivation of photometric phase curves, observations made at different phase angles should be reduced to a standard geometry by using a proper spin and shape model for the object. Such models are, however, rarely available for TNOs. In practice, assuming a linear phase-curve dependence, the phase coefficient and the rotation period are simultaneously derived from minimization of lightcurve scatter. Such an approach provides only rough estimates for phase coefficients. The subsequent step comprises a recomputation of the phase curve by using well-defined lightcurves. However, when a composite lightcurve is based on short-term observations at different phase angles, it is hard to distinguish between the effects from rotation and varying phase angle. In that case, the recalculated phase coefficient is always very close to its rough estimate used for the period determination and remains uncertain.

2.1.3. Small-phase-angle effects in lightcurves. The photometric observations available for KBOs have demonstrated rather large increases in brightness toward the zero phase angle, with rapidly increasing steepness of the phase curve. When studying the lightcurve variations due to rotation, the phase effects need to be taken into account (see chapter by Sheppard et al.). Usually, a linear magnitude phase dependence is assumed, which can be used only as

a rough approximation at phase angles far from the opposition surge. When observations are available at phase angles $\alpha < 0.2°$, great caution is in place when including them in the construction of composite lightcurves. As in the case of Varuna (*Belskaya et al.,* 2006), the opposition surge can reach the amplitude of 0.2 mag relative to the extrapolation from the linear fit of the phase curve at $\alpha > 0.2°$. Omission of the opposition surge will result in an overestimation of the lightcurve amplitude, when observations at extremely small phase angles are included in lightcurve analyses.

Variations of scattering properties over the TNO surfaces can also influence the lightcurve shape and amplitude. Differences both in the amplitude and the positions of lightcurve extrema measured at extremely small (0.1°) and somewhat larger (1°) phase angles were found for Varuna (*Belskaya et al.,* 2006). A plausible explanation for the lightcurve changes is the variation of the light-scattering properties over the surface, giving rise to differing opposition surges, e.g., between two hemispheres of the object. In this case, lightcurves measured at phase angles beyond the opposition surge can be different from those obtained at extremely small phase angles. Generally, the phase effect results in an increase of the lightcurve amplitude toward the zero phase angle, and may give rise to misinterpretations of the rotational properties of KBOs. On the other hand, the study of the amplitude-phase relationship can give additional information on the physical characteristics of the surface.

2.2. Advances in Polarimetry

2.2.1. Principles. In general, the polarization state of light can be fully described by the Stokes vector S (I, Q, U, V) where I is the intensity, Q and U characterize the linear polarization state, and V describes the circular polarization state. Sunlight scattered by solid planetary surfaces (or dust clouds) becomes partially linearly polarized. Two quantities are used to describe the linear polarization state, the total degree of linear polarization P and the position angle θ. The total linear-polarization degree P is equal to $(I_{max} - I_{min})/(I_{max} + I_{min})$, where I_{max} and I_{min} are respectively the maximum and minimum intensities of the polarized light. The position angle θ corresponds to the plane of I_{max}, and is measured with respect to the celestial coordinate system from the direction of the north celestial meridian. These quantities are related to the Stokes parameters

$$P = \sqrt{q^2 + u^2},\ \theta = \frac{1}{2}\arctan\frac{u}{q}$$

where u = U/I and q = Q/I are the normalized Stokes parameters.

For sunlight scattered by planetary surfaces, the polarization plane position is usually either normal or parallel to the scattering plane (the Sun-object-Earth plane). Therefore the polarization degree can be expressed through $P_r = P\cos(2\theta_r)$, where θ_r is the angle between the measured position angle of polarization θ and the normal to the scattering plane: $\theta_r = \theta - (\varphi \pm 90°)$. The angle φ is the position angle of the scattering plane and the sign inside the bracket is chosen to ensure the condition $0° \le (\varphi \pm 90°) \le 180°$. The degree of linear polarization P_r may also be expressed with the help of the intensities scattered perpendicular $I_\perp$ or parallel $I_\parallel$ to the scattering plane

$$P_r = (I_\perp - I_\parallel)/(I_\perp + I_\parallel)$$

It means that the sign of the polarization degree can be positive or negative depending on which component predominates. Negative linear polarization was first discovered by *Lyot* (1929) for the Moon and later found to be a ubiquitous phenomenon for planetary surfaces and interplanetary dust at small phase angles. The degree of polarization varies with the phase angle of observations (the angle between the incident and emergent light) and with the wavelength of the observations, characterizing the properties of the surface, mainly its albedo and texture.

Typical polarization phase curves $P(\alpha)$ of atmosphereless bodies have a negative polarization branch reaching $P_{min} \sim -0.2$ to 2% at phase angles $\alpha_{min} \sim 7°–10°$ turning to positive values at the inversion angle $\alpha_{inv} \sim 20°–25°$ (see, e.g., *Levasseur-Regourd and Hadamcik,* 2003). Most of the polarization phase curves observed have rather symmetric negative branches with $\alpha_{min} \sim \alpha_{inv}/2$ and P near zero at phase angles reaching 0°. For very bright surfaces, an asymmetric peak of negative polarization of about 0.4% has been found at small phase angles of less than 1°–2° (*Rosenbush et al.,* 1997, 2005).

2.2.2. Instrumentation and data reduction. At small phase angles (as observable from the Earth), TNOs are expected to present a relatively small polarization degree. To measure it with an accuracy better than 0.1%, the signal-to-noise ratio needs to be better than 500, which can be achieved only by using large telescopes for these faint objects. At present, all observations available for TNOs and one Centaur have been made with the 8.2-m Very Large Telescope (VLT) in Cerro Paranal Observatory (Chile) using the Focal Reducer/Low Dispersion Spectrograph (FORS1) instrument in its imaging polarimetry mode. Polarimetric observations and data reduction are discussed in detail by *Bagnulo et al.* (2006). A thorough error analysis for dual-beam optical linear polarimetry is given by *Patat and Romaniello* (2006).

2.2.3. Results. The first polarimetric observations for a TNO (except Pluto) were carried out in 2002 by *Boehnhardt et al.* (2004). Observations of the Plutino (28978) Ixion have shown rather pronounced negative polarization noticeably changing as a function of the phase angle in spite of the small range of phase angles covered (0.2°–1.3°). These observations have demonstrated the capability of the polarimetric technique to study distant objects even if they are observable only at very small phase angles, below α_{min}. Later, three additional objects have been observed: (2060) Chiron and (50000) Quaoar (*Bagnulo et al.,* 2006) and 29981 (1999 TD_{10}) (*Rousselot et al.,* 2005b).

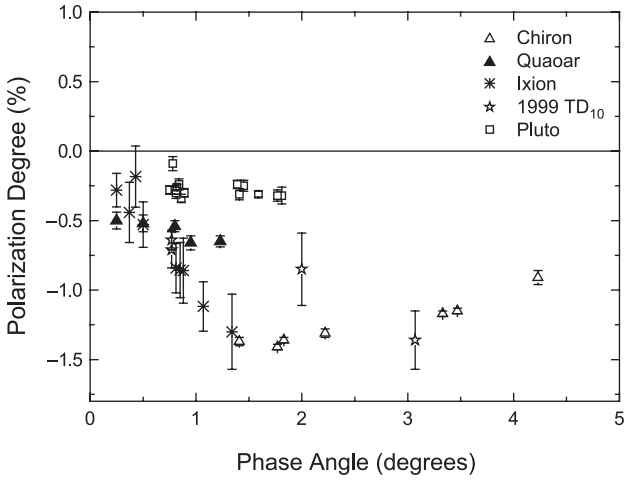

Fig. 2. Polarization phase curves in the R band of KBOs, Centaur Chiron, and for Pluto in the V band (see text for references).

The polarimetric observations available for three KBOs and one Centaur are shown in Fig. 2, which also includes polarimetric data for Pluto, obtained by a number of authors (*Fix and Kelsey,* 1973; *Breger and Cochran,* 1982; *Avramchuk et al.,* 1992). Pluto's polarization curve exhibits a behavior characterized by shallow and nearly constant negative polarization. Although only a few KBOs or Centaurs have been observed up to now, polarimetric observations provide unequivocal evidence for their differing phase curves. Table 2 presents the maximal absolute values of polarization degree $|P_R|$ measured for each object, their geometric albedos p in the R band, and the range of phase angles covered by the observations. The observational data available can be summarized as (1) a noticeable negative polarization is inherent in the surfaces of all distant objects observed, varying from –0.3% to –1.4%; (2) two different polarimetric trends are seen at small phase angles: slow changes in the negative polarization degree for the largest objects (Pluto and Quaoar) and a rapid increase (in absolute terms) in the negative polarization of ~1%/deg in the phase-angle range of 0.3°–1.3° (Ixion); (3) the minimum of the negative polarization branch of Chiron occurs at small phase angles less than 2°; and (4) no wavelength dependence of the polarization degree (BVR bands) is observed for Chiron; a color effect (VR bands) is suspected for 1999 TD_{10}, but its confirmation would require more observations.

3. SIMULATIONS OF PHOTOMETRIC AND POLARIMETRIC OPPOSITION PHENOMENA

3.1. Physical Mechanisms

When considering the physical mechanisms causing the photometric and polarimetric phase dependences, we assume that the TNOs have no noticeable atmospheres that could influence such dependences. This may not always be true. For instance, unusual photopolarimetric properties of Pluto might be partially attributed to its thin atmosphere. Nevertheless, we here ignore possible atmospheric contributions, since there is little data on the atmospheres of TNOs.

There are several physical mechanisms relevant for particulate media that may potentially contribute to the opposition effect. Their contribution depends on the physical parameters of the surface that scatters light, e.g., particle size or porosity. For the surfaces of atmosphereless solar system objects, two main mechanisms are usually considered to be relevant: the shadow-hiding (SM) and coherent-backscattering mechanisms (CBM). Moreover, single-particle scattering also contributes to the opposition phenomena, providing broad backscattering peaks and negative polarization branches (e.g., *Shkuratov et al.,* 2002, 2006; *Muinonen et al.,* 2007). However, single-particle scattering can be envisaged to have a minor direct contribution at small phase angles. In the case of KBOs, SM and CBM are the most important physical mechanisms for the phenomena. Note that, on one hand, SM contributes to the photometric phase dependencies only. On the other hand, CBM contributes both to photometric and polarimetric phase dependencies. Below, we briefly describe both mechanisms. More details can be found in the reviews by *Muinonen* (1994) and *Shkuratov et al.* (2002).

3.1.1. Coherent backscattering mechanism. In order to describe the mechanism, let us consider an incident electromagnetic plane wave (wavelength λ and wave number $k = 2\pi/\lambda$) propagating in the negative direction of the z-axis and interacting with two end scatterers A and B, which are on

TABLE 2. Polarization degree measured for KBOs and a Centaur.

Object	p_R*	Phase-angle Range (deg)	$\lvert P_R\rvert$ (%)	Reference
(2060) Chiron	0.08	1.41–4.23	1.40	*Bagnulo et al.* (2006)
(28978) Ixion	0.20	0.25–1.34	1.30	*Boehnhardt et al.* (2004)
(29981) 1999 TD_{10}	0.05	0.77–3.10	1.35	*Rousselot et al.* (2005b)
(50000) Quaoar	0.26	0.25–1.23	0.65	*Bagnulo et al.* (2006)
(134340) Pluto	0.61†	0.75–1.81	0.32†	*Breger and Cochran* (1982); *Fix and Kelsey* (1973)

*Albedo is given according to Stansberry et al. (this volume).
†Data are given for the V band.

the order of one to hundreds of wavelengths apart, via an arbitrary number of intermediate scatterers in between them. Two scattered wave components due to the two opposite propagation directions between scatterers A and B always interfere constructively in the backward direction, whereas in other directions, the interference characteristics vary. Three-dimensional averaging over scatterer locations results in a backscattering enhancement with decreasing angular width for increasing number of intermediate scatterers, because the average distance between the end scatterers is larger for higher numbers of intermediate scatterers.

In order to explain the CBM for the negative degree of linear polarization for unpolarized incident light, the derivation and proper averaging of the Stokes vectors corresponding to the scattered electromagnetic fields are required for two orthogonal linear polarization states of the incident plane wave. Consider incident polarizations parallel and perpendicular to the scattering plane (here yz-plane) defined by the light source, object, and the observer. For simplicity, consider two scatterers A and B at a distance d from one another aligned either on the x-axis or the y-axis, while the observer is in the yz-plane. Since first-order scattering is typically positively polarized (e.g., Rayleigh scattering and Fresnel reflection), the scatterers sufficiently far away from each other ($kd = 2\pi d/\lambda \gg 1$) interact predominantly with the electric field vector perpendicular to the plane defined by the source and the two scatterers, while interaction with the electric field vector parallel to that plane is suppressed. The observer in the yz-plane will detect negative polarization from the geometry with the scatterers aligned along the x-axis and the incident polarization along the y-axis, and positive polarization from the geometry with the scatterers aligned along the y-axis and the incident polarization along the x-axis. However, the positive polarization suffers from the phase difference $kd \sin\alpha$, whereas the phase difference for the negative polarization is zero for all phase angles. Averaging over scatterer locations will result in negative polarization near the backward direction. Scattering orders higher than the second, which experience similar preferential interaction geometries, can also contribute to negative polarization. As above for the opposition effect, the contributions from increasing orders of scattering manifest themselves at decreasing phase angles.

3.1.2. Shadowing mechanism. On the surfaces of TNOs, SM is bound to be relevant for length scales significantly larger than the wavelength of incident light. It is the most prominent first-order scattering mechanism. In principle, we can distinguish between shadowing by the rough interface between the regolith and the free space and shadowing by the internal geometric structure of the regolith, whereas in practice, for disk-integrated photometric data, it can be difficult if not impossible to discriminate between the two shadowing contributions. In both cases, SM is due to the fact that a ray of light penetrating into the scattering medium and incident on a certain particle can always emerge back along the path of incidence, whereas in other directions, the emerging ray can be blocked by other particles. The internal SM depends mainly on the volume density of the scattering medium, whereas the interfacial SM depends mainly on surface roughness (here standard deviation of the interfacial slopes). Recent studies of the internal SM and interfacial SM have been carried out by, e.g., *Muinonen et al.* (2001), *Shkuratov et al.* (2005), and *Parviainen and Muinonen* (2007).

3.1.3. Analytical models. There are no rigorous electromagnetic solutions for light scattering by random rough surfaces, whereas in specific cases, analytical approximations are available for, e.g., the interpretation of photometric observations. The most popular model is the photometric model proposed by *Hapke* (1986). It accounts for (1) single-particle scattering, (2) shadowing due to particulate surfaces and their large-scale topography, and (3) multiple scattering between the particles. The model was later modified to incorporate coherent backscattering and the influence of anisotropic single scatterers on multiple scattering, with seven free parameters in the latest version (*Hapke,* 2002). Unfortunately, the theory does not allow an unambiguous interpretation of observed or measured phase curves. Even for asteroids observed at large ranges of phase angles, the Hapke model does not give reliable estimates for photometric parameters (see *Helfenstein and Veverka,* 1989). Besides, the model incorporates the so-called diffusion approximation to describe coherent backscattering, which cannot be applied in the case of particulate surfaces with low and intermediate albedo. Moreover, any coherent backscattering model has to take into account polarization in order to correctly describe the photometric spike (*Mishchenko,* 1991); the Hapke model is a scalar one and does not consider polarization at all.

Mishchenko et al. (2000) made use of the analytical theories by *Ozrin* (1992) and *Amic et al.* (1997) to compute coherent backscattering by nonabsorbing media of Rayleigh scatterers. They were able to offer reference results, i.e., accurate predictions for the values of the amplitude and width of the opposition effect and the shape and depth of the negative polarization surge. One of the main predictions is that the photometric opposition effect is accompanied by a polarization opposition effect of the same angular width (e.g., *Mishchenko and Dlugach,* 1993). There are, however, several shortcomings in the approach by *Mishchenko et al.* (2000): (1) absorbing scatterers are not treated; (2) the results are limited to Rayleigh scatterers; and (3) the shadowing effects are excluded.

3.2. Numerical Modeling

The backscattering phenomena can be studied using Monte Carlo (MC) simulations of radiative transfer and coherent backscattering for particulate surfaces of spherical scatterers (*Shkuratov et al.,* 2002; *Muinonen,* 2004). The application of MC modeling to the polarimetric and photometric observations is bound to require certain simplifications. For example, the single scatterers are assumed to be Rayleigh-scatterers (e.g., *Muinonen et al.,* 2002), allowing simultaneous modeling of the photometric and polarimetric phase effects using a minimum number of physical parameters, i.e., the single-scattering albedo and mean free

path. The MC method for coherent backscattering by absorbing and scattering media mimics radiative transfer but, for each multiple-scattering event, it additionally computes the coherent-backscattering contribution with the help of the reciprocity relation in electromagnetic scattering. Application of the Rayleigh-scatterer model to the observations of KBOs and one Centaur showed that a possible way to explain their polarization properties is to assume two-component surface media consisting of Rayleigh scatterers with small and large single-scattering albedos. Details of model fits are given in *Boehnhardt et al.* (2004), *Bagnulo et al.* (2006), and *Rousselot et al.* (2005b). Note that the fits are by no means unambiguous; rather, they demonstrate the capability of the two-component model to explain the observations. Moreover, the model considers the geometric albedo as a parameter known *a priori*, e.g., from thermal infrared observations. Since the present KBO albedos are poorly known, potential changes in them can imply changes in the parameters of the two-component model [cf. Ixion (*Bagnulo et al.,* 2006)].

Polarimetric observations of bright objects like Pluto are difficult to explain using a Rayleigh-scatterer model. This is in agreement with the findings in *Muinonen et al.* (2002) for bright asteroids. However, the Rayleigh-scatterer model that includes a coherent-backscattering component with a long mean free path is capable of explaining the observations. Clearly, a more sophisticated scatterer model in coherent backscattering could allow more significant CBM contributions to the opposition effect.

There are some intriguing features predicted by the modeling of the observations available for KBOs. Figure 3 shows model phase curves of brightness and polarization for Chiron, Ixion, and Pluto. The modeling suggests a narrow spike in both polarimetry and photometry for all objects that can be checked with future observations. We emphasize that a sharp surge in brightness and polarization at phase angles less than 0.2° is also suggested for Pluto. Further discussion will be given in section 4. Here we would like to emphasize that detailed phase curves for both brightness and polarization are a necessity for further progress in modeling and that observations at phase angles very close to zero are crucial for verifying the coherent-backscattering contributions.

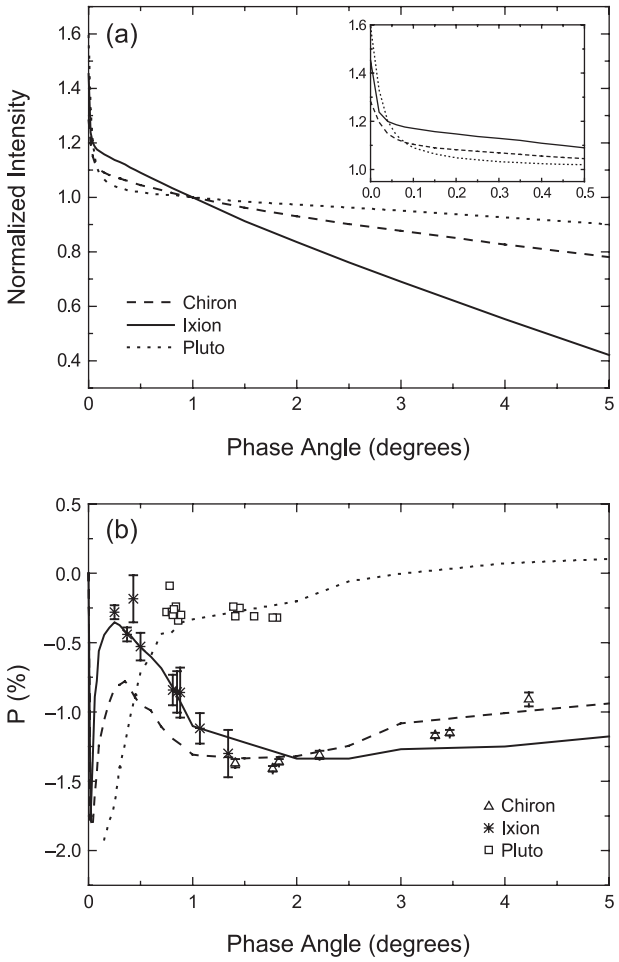

Fig. 3. Examples of **(a)** model intensity and **(b)** polarization fits for Chiron, Ixion, and Pluto. The inset in the upper corner of **(a)** shows the small phase angle region in greater detail. The available polarimetric observations of these objects are also plotted (see text for references).

3.3. Laboratory Simulations

3.3.1. Instruments for experimental simulations. In order to be applicable to the interpretation of KBO observations, laboratory measurements should be carried out down to very small phase angles. Measurements at such phase angles are technically difficult and require special instruments. For that very purpose, a new laboratory photometer was designed at the Institute of Astronomy of Kharkiv National University to perform measurements in the phase-angle range of 0.008°–1.5°. Such small phase angles become feasible due to the small linear apertures of the light source (unpolarized laser) and the receiver, and the large distances from the scattering sample surface to the light source and the detector (*Psarev et al.,* 2007). The new device complements the other Kharkiv laboratory photopolarimeter, which works in the phase-angle range of 0.2°–17° and uses a lamp as the light source (*Shkuratov et al.,* 2002). Numerous small-phase-angle measurements were also made at the Jet Propulsion Laboratory (JPL) using the long-arm goniometric photopolarimeter with a laser as the light source, covering the phase-angle range of 0.05°–5° (*Nelson et al.,* 2000). The Kharkiv and JPL instruments were intercalibrated by measuring the same sample. A laboratory instrument suitable for photometric measurements down to the phase angle of 0.2° was used at the University of Helsinki Observatory with an unpolarized laser (*Kaasalainen et al.,* 2002). The laboratory experiments were also made to simulate polarimetric properties of both regoliths and dust clouds under microgravity conditions (e.g., *Levasseur-Regourd and Hadamcik,* 2003).

3.3.2. Brightness opposition spike. A key question to be answered by the laboratory measurements is: Which surfaces can produce narrow and sharp brightness opposi-

tion spikes? The opposition spike is found to be more prominent with increasing surface albedo (e.g., *Shkuratov et al.,* 2002; *Psarev et al.,* 2007). Results from photometric measurements in the phase-angle range of 0.008°–1.5° for two samples with substantially differing albedos, a very bright sample of smoked MgO and a very dark sample of carbon soot, are shown in Fig. 4. For both samples, thick layers of smoked materials were used, and both surfaces were very fluffy. Results shown in Fig. 4 allow one to compare data obtained with the Kharkiv lamp and laser photometer at the equivalent wavelength of 0.63 μm. The curves for the same sample measured by different instruments are in good agreement. The bright and dark samples have albedos of 99% and 2.5%, respectively, determined at a 2° phase angle relative to the photometric standard Halon. The MgO sample has a very prominent opposition spike at phase angles <0.8°. The dark sample of carbon soot does not show any significant opposition features with an almost linear phase dependence in the range of 0.008°–2°. However, if we consider a wider phase-angle range up to 15°, the nonlinearity of the carbon-soot phase curve can be clearly seen (Fig. 4). The laboratory data suggests that surfaces giving rise to the opposition spike have inevitably rather high albedos necessary to produce the coherent-backscattering enhancement. Further measurements of mixtures of MgO and carbon soot samples in various proportions (albedos 9%, 19%, 47%) have shown that the opposition spike becomes noticeable for albedos greater than 19% (*Psarev et al.,* 2006). It was also shown that the width of the spike depends on the surface texture, mainly its packing density.

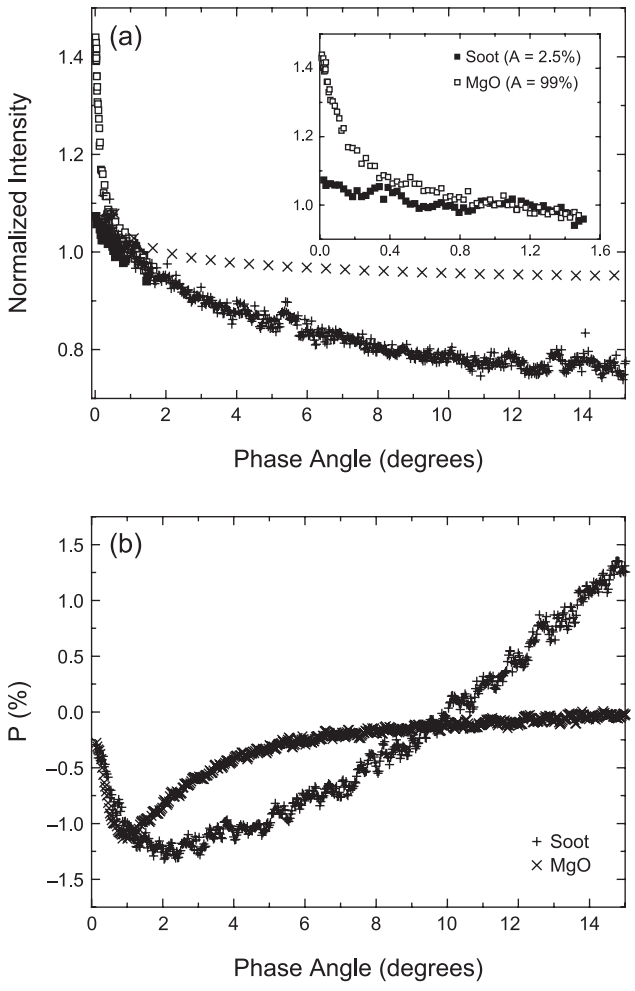

Fig. 4. **(a)** Photometric and **(b)** polarimetric phase curves for MgO measured with the laser laboratory photometer (open and filled squares) and the lamp photopolarimeter (crosses and pluses). The inset in the upper corner of **(a)** shows the small phase angle region in greater detail.

Thus, laboratory measurements suggest that observations of the opposition spike can put constraints on the surface albedo and texture. In particular, a very narrow and sharp opposition spike observed for Varuna and probably for other KBOs could indicate rather high surface albedos and a fluffy surface texture.

3.3.3. Negative polarization. The first polarimetric observations of three KBOs and one Centaur raise two main questions, insofar as laboratory measurements are concerned: (1) Which surface properties influence the position of the minimum polarization, and (2) which surfaces can produce a significant negative polarization at small phase angles?

Numerous laboratory polarimetric measurements have been carried out to study negative polarization (for surveys see *Muinonen et al.,* 2002; *Shkuratov and Ovcharenko,* 2002). The depth and shape of the negative-polarization branch was found to depend strongly on such parameters as complex refractive index, particle size, packing density, and microscopic optical heterogeneity of the laboratory samples, all affecting the albedo of the surface. An attempt to distinguish the effects of individual surface parameters on the photometric and polarimetric phase curves was made by *Shkuratov et al.* (2002) based on the laboratory measurements of diverse samples in the phase-angle range of 0.2°–4°. Here we briefly summarize the current understanding of the roles of the abovementioned parameters in the formation of the negative-polarization branch.

3.3.4. Albedo. Although the geometric albedo of the surface follows from the physical parameters, it is valuable to summarize certain empirical relations including the albedo as one of the parameters. The inverse correlation between the albedo and the maximum of the negative polarization degree (in absolute terms) is usually observed for pulverized silicates and meteorites (e.g., *Zellner et al.,* 1977). As a rule, the lower the albedo, the deeper the negative polarization branch. The correlation is successfully applied in the estimation of geometric albedos for asteroids. It is not yet known whether it can be applied to KBOs and Centaurs. At small phase angles, the correlation is destroyed by the interplay of the physical parameters of the surfaces (*Shkuratov et al.,* 2002).

3.3.5. Refractive index. The real part of the refractive index affects the shape of the negative-polarization branch. Increasing the real part usually makes the negative polar-

ization branch more prominent. The imaginary part of the refractive index affects primarily the albedo of the surface (see above).

3.3.6. Particle size. An increase in the depth of negative polarization is observed for powdered dielectric surfaces with decreasing particle size down to the wavelength of incident light. It is well illustrated by laboratory measurements of particle-size separates of bright powders of Al_2O_3 made by *Shkuratov et al.* (2002). For grain sizes larger than 1 μm, the depth of the negative-polarization branch does not effectively exceed 0.25%. However, the smallest particle fractions of 0.1 μm and 0.5 μm show astonishingly similar negative-polarization branches with the minimum of about 0.8% situated at $\alpha \sim 1.6°$. Qualitatively, the measurements reproduce the polarimetric features of KBOs suggesting that their surfaces include a large portion of submicrometer- to micrometer-sized particles. In fact, a pronounced negative polarization is typical of granular structures in 1-μm size scales and of complex small-scale topographies. Measurements of the fine SiO_2 powder with fractal-like structures, where tiny particles (~10 nm) form aggregates and the aggregates form larger aggregates, etc., shows an extremely narrow negative polarization branch (Fig. 5).

3.3.7. Packing density. Measurements of laboratory samples of fine dispersed particles before and after compression clearly show differing phase-angle dependences (Fig. 5). Fluffy samples of MgO powder (~1 μm) and superfine SiO_2 powder (~10 nm) produce asymmetric negative polarization branches with minima at small phase angles. After compressing, the negative-polarization branch became wider. Details of the measurements are given in *Shkuratov et al.* (2002).

3.3.8. Microscale optical heterogeneity. Optically contrasting media give rise to pronounced negative-polarization branches. A significant increase of negative polarization (in absolute terms) is found when fine powders with highly different albedos are mixed together (*Shkuratov,* 1987). Even small amounts of a bright powder added to a dark powder (e.g., a mixture of 5% of MgO and 95% of carbon soot) noticeably increase the negative polarization as compared to that of the individual mixture components. Laboratory measurements reproducing phase curves of cometary dust also require mixtures of bright and dark fluffy materials to obtain relevant negative-polarization branches (*Hadamcik et al.,* 2006).

3.3.9. Interrelations between the negative-polarization branch and the opposition effect. In many cases, the parameters of the opposition effect and the negative-polarization branch are closely correlated. Generally, the opposition effect becomes more prominent with increasing surface albedo whereas the negative-polarization branch is neutralized. However, there are a number of exceptions to the typically observed relationships between the opposition effect and the negative-polarization branch (for details see *Shkuratov et al.,* 2002). This conclusion is well-illustrated in Figs. 4–5, which show both brightness and polarization measurements for carbon soot, MgO, and SiO_2. One can see that there is no strict correlation between the photometric and polarimetric phase dependences.

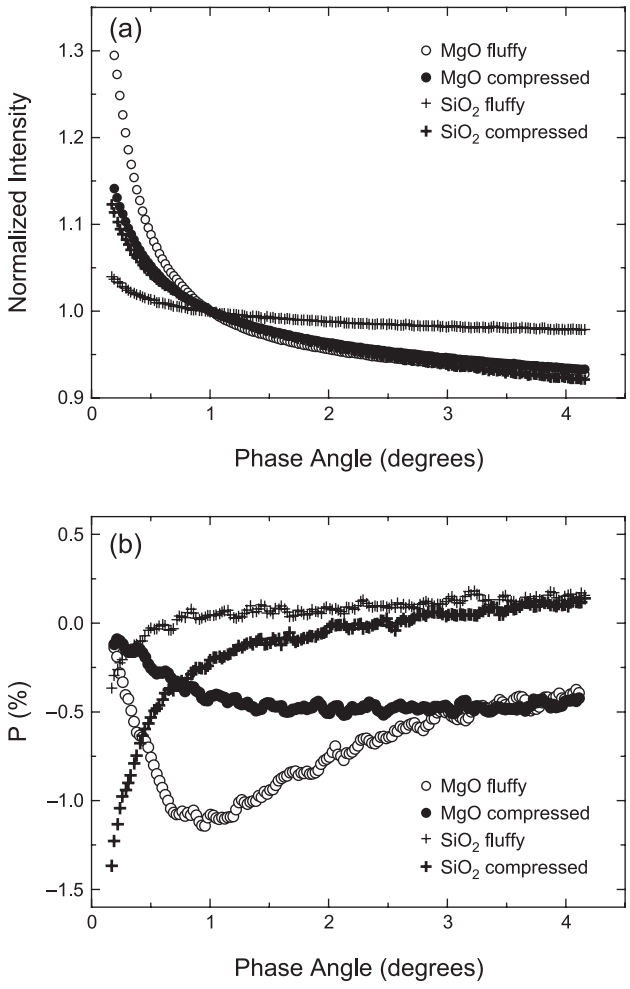

Fig. 5. **(a)** Photometric and **(b)** polarimetric phase curves for MgO and SiO_2 before and after compressing with alcohol drying at $\lambda = 0.63$ μm (*Shkuratov et al.,* 2002).

4. DISCUSSION AND CONCLUSIONS

The first observations of the phase-angle effects in brightness and polarization for KBOs and Centaurs underscore their significance in constraining the albedos and surface textures of these objects. In spite of the limited range of phase angles accessible from groundbased observations, distinct features have been observed both in brightness and polarization. Their interpretation based on numerical and laboratory simulations may suggest the following surface properties: (1) fluffy surfaces with a large portion of submicrometer- or micrometer-sized particles; (2) inhomogeneous surface matter (scatterers with small and large single-scattering albedos); (3) moderate to high albedos of surfaces showing sharp opposition spikes. Note that fluffy surfaces are possible but not necessary, e.g., similar phase effects can arise when shadowing and coherent backscattering take

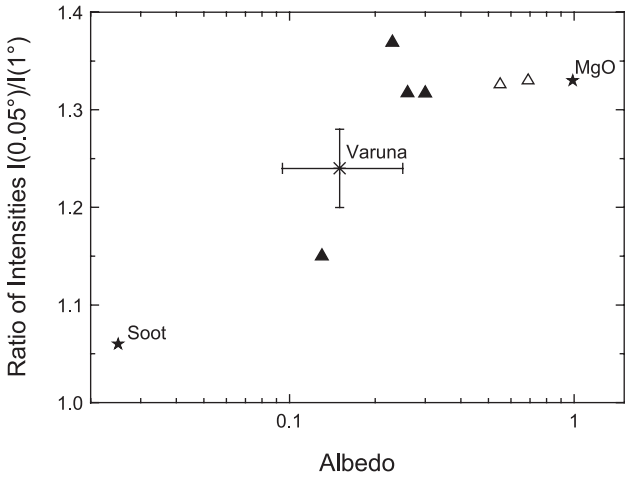

Fig. 6. Ratio of intensities at the phase angle of 0.05° to that at the phase angle of 1° for uranian satellites (black triangles), saturnian satellites (open triangles), TNO Varuna, and the laboratory samples.

place among scatterers embedded in an otherwise optically homogeneous host material.

Additional constraints on the surface properties can be derived from the comparison of the observational features obtained for KBOs and Centaurs with the corresponding features for other solar system objects. Phase curves near opposition have been measured for a variety of solar system objects. In spite of the different compositions and origins, most of the objects give rise to rather similar photometric and polarimetric characteristics mainly depending on surface albedo. The comparison suggests a way to constrain the surface albedo by using small-phase-angle observations. Figure 6 shows the ratio of intensities measured at $\alpha = 0.05°$ to that at $\alpha = 1°$ for both laboratory samples and planetary surfaces. Data of uranian and saturnian satellites were taken according to *Buratti et al.* (1992) and *Verbiscer et al.* (2005), respectively. Note that we are using only data obtained at these small phase angles avoiding any model-dependent extrapolations. Observations of main-belt asteroids cannot be used in such a comparison due to the influence of the finite angular size of the solar disk. The data of the uranian and saturnian satellites were taken from *Buratti et al.* (1992) and *Verbiscer et al.* (2005), respectively. The ratio of I(0.05°)/I(1°) tends to increase with surface albedo and seems to saturate for albedos of 30–40%, when further increasing of albedo does not change the ratio. This is likely to be connected to the usage of 0.05° as the limiting phase angle for the ratio estimations. Good coincidence of the laboratory data and available telescopic observations suggests a similarity of the surface textures of the smoked samples to those of the satellites and the TNO Varuna. The ratio of I(0.05°)/I(1°) observed for Varuna is typical for moderate-albedo surfaces.

The phase coefficients of atmosphereless bodies estimated at larger phase angles usually exhibit a simple relation to albedo: The higher the phase coefficient, the lower the surface albedo (e.g., *Belskaya and Shevchenko,* 2000). It can be explained by the dominant influence of the shadowing mechanism on the phase curves at phase angles beyond the opposition surge. A similar trend could exist for the TNO and Centaur phase coefficients as pointed out by *Rousselot et al.* (2006) and *Rabinowitz et al.* (2007). Further observations are needed to confirm the trend.

Many observers have mentioned the large phase coefficients measured for Centaurs and TNOs. An important question is whether they really differ from those of other solar system objects. Unfortunately, uncertainties in the phase-coefficient estimation in the limited phase-angle range of TNOs are so large that no conclusions can be currently made. However, the phase-coefficient determinations for Centaurs up to the phase angles of 4°–7° provide irrefutable evidence of a larger steepness of their phase curves as compared to those of other solar system objects. As one can see from Fig. 7, the ratios of intensities I(1°)/I(4°) measured for Centaurs are considerably larger than those of other objects. A possible correlation of the phase coefficient with the albedo needs to be verified with additional observations.

A pronounced branch of negative polarization deeper than 1% at small phase angles close to 1° is also unique among solar system bodies observed so far. At such small phase angles, the polarization degree typically does not fall below –0.6% for a variety of minor bodies (asteroids, cometary dust, satellites of major planets), being almost independent of their surface albedos (Fig. 8). The observations available for the KBOs and the one Centaur do not yet allow to conclude whether we have observed a "normal" negative branch of polarization or an additional narrow peak predicted by theoretical modeling of coherent backscattering (e.g., *Mishchenko et al.,* 2000). *Rosenbush et al.* (1997, 2005) claimed a detection of such a peak in the observations

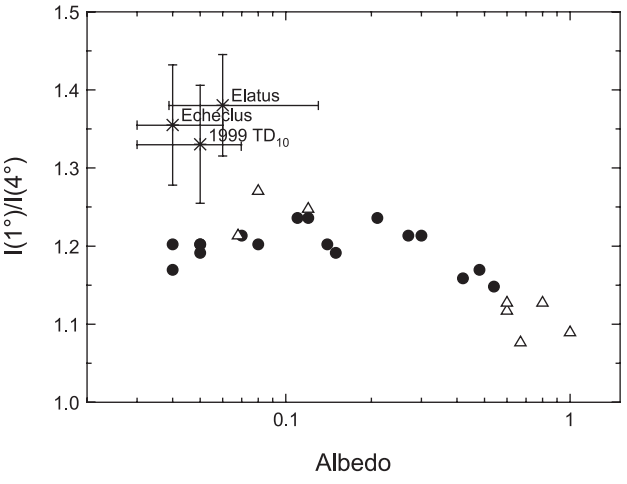

Fig. 7. Phase coefficient vs. albedo for asteroids, satellites (triangles), and Centaurs. For references for asteroid and satellite data, see *Belskaya and Shevchenko* (2000) and *Bauer et al.* (2006). Albedos of Centaurs were taken from Stansberry et al. (this volume).

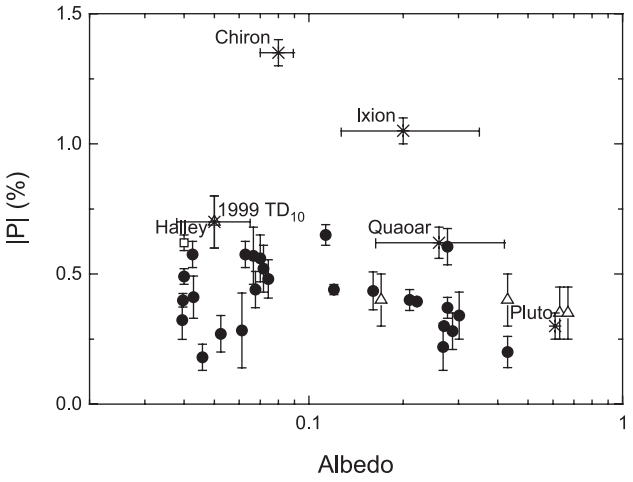

Fig. 8. Polarization degree at $\alpha = 1°$ vs. albedo for asteroids (circles) from *Cellino et al.* (2005) and *Fornasier et al.* (2006), satellites (triangles) from *Rosenbush et al.* (1997), a comet from *Kiselev et al.* (2005), and TNOs (for references see text).

of bright satellites and asteroids but its small depth (typically less than 0.4%) together with the large scatter of data raise doubts about its existence. Observations of moderate- and low-albedo asteroids did not show any particular features at small phase angles (e.g., *Cellino et al.,* 2005). Numerical modeling (see section 3.2) has suggested a secondary peak of polarization for Chiron, Ixion, and Pluto, which are important to verify with future observations.

An alternative explanation is that the polarization phase dependences of KBOs and Centaurs are extremely asymmetric and, thus, the phase angle, at which P_{min} is observed, is close to 1°–2°. This may explain the trend seen between the albedo and the negative polarization degree for the KBOs and Centaur observed (Fig. 8), resembling that for asteroids. Further observations of objects with known albedos are needed to study whether the trend really exists. If confirmed, it may allow an independent estimation of surface albedos based on polarimetric observations.

Note that the negative branches of polarization measured for a few comets (*Kiselev et al.,* 2005) are, in general, quite similar to those of low-albedo asteroids while they are more symmetric. The phase angle of the minimum polarization for S-type asteroids is systematically smaller than that of cometary dust (see, e.g., *Levasseur-Regourd,* 2004).

Although reliable observational data on phase effects in photometry and polarimetry are very scarce for KBOs and Centaurs, the existing data give a first look into the microscopic properties of the surface layers and suggest different surface properties as compared to less distant small solar system objects.

The study of the photometric and polarimetric phase effects for KBOs and Centaurs is just beginning. The available observations have revealed remarkable features in the opposition brightening and negative polarization that can be used to constrain surface properties on these distant objects. Further photometric and polarimetric observations are needed to understand how common the features are and to probe the differences in surface properties of objects having different dynamical histories. Special observation programs of objects with well-determined albedos can help to establish possible empirical correlations between the photometric and polarimetric parameters and the geometric albedo of the surface. Storage of the original photometric observations of KBOs and Centaurs is of great importance since it allows the compilation of all data from different observers and the subsequent new interpretations of the phase curves. Such a database was initiated by Rousselot et al. (*www.obs-besancon.fr/bdp/*). Finally, it is important to develop a new empirical system to compute absolute magnitudes for KBOs: the H, G magnitude system fails to fit the photometric phase curves.

Further progress in remote sensing of the surface properties requires further developments in theoretical and numerical modeling, and laboratory simulations of light scattering. Numerical modeling is able to give predictions that need to be checked by further observations. Detailed observations of polarimetric and photometric phase curves down to extremely small phase angles are of great value to improve the theoretical models. Only close coordination of observations and modeling can provide further progress in obtaining meaningful results on surface textural properties from remote-sensing data. Moreover, an extension of the spectral range of observations and using other types of measurements for joint analyses (e.g., spectroscopy, radiometry) is a promising way to improve our knowledge on the surface properties of KBOs and Centaurs.

Acknowledgments. We thank A. Verbiscer and A. Ovcharenko for providing us with important unpublished data and A. Cellino and Yu. Krugly for valuable comments. I.B. and Yu.S. are grateful to Université Pierre et Marie Curie for financing their stay in France. K.M. is grateful to the Academy of Finland for partial funding of his research.

REFERENCES

Amic E., Luck J. M., and Nieuwenhuizen Th. M. (1997) Multiple Rayleigh scattering of electromagnetic waves. *J. Phys. I, 7,* 445–483.

Avramchuk V. V., Rakhimov V. I., Chernova G. P., and Shavlovskii N. M. (1992) Photometry and polarimetry of Pluto near its perihelion. *Kinemat. Fiz. Nebesn. Tel, 8(4),* 37–45 (in Russian).

Bagnulo S., Boehnhardt H., Muinonen K., Kolokolova L., Belskaya I., and Barucci M. A. (2006) Exploring the surface properties of Transneptunian Objects and Centaurs with polarimetric FORS1/VLT observations. *Astron. Astrophys., 450,* 1239–1248.

Bauer J. M., Meech K. J., Fernandez Ya. R., Farnham T. L., and Roush T. L. (2002) Observations of the Centaur 1999 UG5: Evidence of a unique outer solar system surface. *Publ. Astron. Soc. Pac., 114,* 1309–1321.

Bauer J., Meech K., Fernandez Y., Pittichova J., Hainaut O., Boehnhardt H., and Delsanti A. (2003) Physical survey of 24 Centaurs with visible photometry. *Icarus, 166,* 195–211.

Bauer J. M., Grav T., Buratti B. J., and Hicks M. D. (2006) The

phase curve survey of the irregular saturnian satellites: A possible method of physical classification. *Icarus, 184,* 181–197.

Belskaya I. N. and Shevchenko V. G. (2000). Opposition effect of asteroids. *Icarus, 147,* 94–105.

Belskaya I. N., Barucci M. A., and Shkuratov Yu. G. (2003) Opposition effect of Kuiper belt objects: Preliminary estimations. *Earth Moon Planets, 92,* 201–206.

Belskaya I. N., Ortiz J. L., Rousselot P., Ivanova V., Borisov G., Shevchenko V. G., and Peixinho N. (2006) Low phase angle effects in photometry of trans-neptunian objects: 20000 Varuna and 1996 TO_{66}. *Icarus, 184,* 277–284.

Binzel R. P. and Mulholland J. D. (1984) Photometry of Pluto during the 1983 opposition — A new determination of the phase coefficient. *Astron. J., 89,* 1759–1761.

Boehnhardt H., Bagnulo S., Muinonen K., Barucci M. A., Kolokolova L., Dotto E., and Tozzi G. P. (2004) Surface characterization of 28978 Ixion (2001 KX_{76}). *Astron. Astrophys., 415,* L21–L25.

Breger M. and Cochran W. D. (1982) Polarimetry of Pluto. *Icarus, 49,* 120–124.

Buie M. W. and Bus S. J. (1992) Physical observations of (5145) Pholus. *Icarus, 100,* 288–294.

Buie M., Tholen D., and Wasserman L. (1997) Separate lightcurves of Pluto and Charon. *Icarus, 125,* 233–244.

Buratti B. J., Gibson J., and Mosher J. A. (1992) CCD Photometry of the uranian satellites. *Astron. J., 104,* 1618–1622.

Buratti B. J., Hillier J. K., Heinze A., Hicks M. D., Tryka K. A., Mosher J. A., Ward J., Garske M., Young J., and Atienza-Rosel J. (2003) Photometry of Pluto in the last decade and before: Evidence for volatile transport? *Icarus, 162,* 171–182.

Cellino A., Gil Hutton R., Di Martino M., Bendjoya Ph., Belskaya I. N., and Tedesco E. F. (2005) Asteroid polarimetric observations using the Torino UBVRI photopolarimeter. *Icarus, 179,* 304–324.

Fix L. A. and Kelsey J. D. (1973) Polarimetry of Pluto. *Astrophys. J., 184,* 633–636.

Fornasier S., Belskaya I., Shkuratov Yu. G., Pernechele C., Barbieri C., Giro E., and Navasardyan H. (2006) Polarimetric survey of asteroids with the Asiago telescope. *Astron. Astrophys., 455,* 371–376.

Hadamcik E., Renard J. B., Levasseur-Regourd A. C., and Lasue J. (2006) Light scattering by fluffy particles with the $PROGRA^2$ experiment: Mixtures of materials. *J. Quant. Spectros. Rad. Transfer, 100,* 143–156.

Hapke B. (1986) Bidirectional reflectance spectroscopy. 4. The extinction coefficient and the opposition effect. *Icarus, 67,* 264–280.

Hapke B. (2002) Bidirectional reflectance spectroscopy. 5. The coherent backscatter opposition effect and anisotropic scattering. *Icarus, 157,* 523–534.

Helfenstein P. and Veverka J. (1989) Physical characterization of asteroid surfaces from photometric analysis. In *Asteroids II* (R. Binzel et al., eds.), pp. 557–593. Univ. of Arizona, Tucson.

Hicks M. D., Simonelli D. P., and Buratti B. J. (2005) Photometric behavior of 20000 Varuna at very small phase angles. *Icarus, 176,* 492–498.

Jewitt D. and Sheppard S. (2002) Physical properties of trans-Neptunian object (20000) Varuna. *Astron. J., 123,* 2110–2120.

Kaasalainen S., Piironen J., Muinonen K., Karttunen H., and Peltoniemi J. I. (2002) Laboratory experiments on backscattering from regolith samples. *Appl. Opt., 41,* 4416–4420.

Kiselev N., Rosenbush V., Jockers K., Velichko S., and Kikuchi S. (2005) Database of comet polarimetry: Analysis and some results. *Earth Moon Planets, 97,* 365–378.

Levasseur-Regourd A. C. (2004) Polarimetry of dust in the solar system: Remote observations, in-situ measurements and experimental simulations. In *Photopolarimetry in Remote Sensing* (G. Videen et al., eds.), pp. 393–410. NATO Sci Series, Kluwer, London.

Levasseur-Regourd A. C. and Hadamcik E. (2003) Light scattering by irregular dust particles in the solar system: Observations and interpretation by laboratory measurements. *J. Quant. Spectros. Rad. Transfer, 79-80,* 903–910.

Lyot B. (1929) Recherches sur la polarisation de la lumière des planètes et de quelques substances terrestres. *Ann. Obs. Paris, 8,* 1–161.

McBride N., Davies J. K., Green S. F., and Foster M. J. (1999) Optical and infrared observations of the Centaur 1997 CU_{26}. *Mon. Not. R. Astron. Soc., 306,* 799–805.

Mishchenko M. I. (1991) Polarization effects in weak localization of light: Calculation of the copolarized and depolarized backscattering enhancement factors. *Phys. Rev., B44,* 12597–12600.

Mishchenko M. I. and Dlugach J. M. (1993) Coherent backscatter and the opposition effect for E-type asteroids. *Planet. Space Sci., 41,* 173–181.

Mishchenko M. I., Luck J.-M., and Nieuwenhuizen T. M. (2000) Full angular profile of the coherent polarization opposition effect. *J. Opt. Soc. Am. A, 17,* 888–891.

Muinonen K. (1994) Coherent backscattering by solar system dust particles. In *Asteroids, Comets, Meteors 1993* (A. Milani et al., eds.), pp. 271–296. IAU Symposium No. 160, Kluwer, Dordrecht.

Muinonen K. (2004) Coherent backscattering of light by complex random media of spherical scatterers: Numerical solution. *Waves Random Media, 14(3),* 365–388.

Muinonen K., Stankevich D., Shkuratov Yu. G., Kaasalainen S., and Piironen J. (2001) Shadowing effect in clusters of opaque spherical particles. *J. Quant. Spectros. Rad. Transfer, 70,* 787–810.

Muinonen K., Piironen J., Shkuratov Yu. G., Ovcharenko A. A., and Clark B. E. (2002) Asteroid photometric and polarimetric phase effects. In *Asteroids III* (W. F. Bottke Jr. et al., eds.), pp. 123–138. Univ. of Arizona, Tucson.

Muinonen K., Zubko E., Tyynelä J., Shkuratov Yu. G., and Videen G. (2007) Light scattering by Gaussian random particles with discrete-dipole approximation. *J. Quant. Spectros. Rad. Transfer, 106,* 360–377.

Nelson R., Hapke B., Smythe W., and Spilker L. (2000) The opposition effect in simulated planetary regolith. Reflectance and circular polarization ratio change at small phase angle. *Icarus, 147,* 545–558.

Ozrin V. D. (1992) Exact solution for coherent backscattering of polarized light from a random medium of Rayleigh scatterers. *Waves Random Media, 2,* 141–164.

Parviainen H. and Muinonen K. (2007) Rough-surface shadowing for self-affine random rough surfaces. *J. Quant. Spectrosc. Radiat. Transfer, 106,* 389–397.

Patat F. and Romaniello M. (2006) Error analysis for dual-beam optical linear polarimetry. *Publ. Astron. Soc. Pac., 118,* 146–161.

Psarev V., Ovcharenko A., Shkuratov Yu., Belskaya I., and Videen G. (2007) Photometry of surfaces with complicated structure at extremely small phase angles. *J. Quant. Spectrosc. Radiat. Transfer, 106,* 455–463.

Rabinowitz D., Barkume K., Brown M., et al. (2006) Photometric observations constraining the size, shape and albedo of 2003 EL_{61}, a rapidly rotating, Pluto-sized object in the Kuiper belt. *Astrophys. J., 639,* 1238–1251.

Rabinowitz D., Schaefer B., and Tourtellote S. (2007) The diverse solar phase curves of distant icy bodies. Part 1: Photometric observations of 18 trans-neptunian objects, 7 Centaurs, and Nereid. *Astron. J., 133,* 26–43.

Rosenbush V. K., Avramchuk V. V., Rosenbush A. E., and Mishchenko M. I. (1997) Polarization properties of the Galilean satellites of Jupiter: Observations and preliminary analysis. *Astrophys. J., 487,* 402–414.

Rosenbush V. K., Kiselev N. N., Shevchenko V. G., Jockers K., Shakhovskoy N. M., and Efimov Yu. S. (2005) Polarization and brightness opposition effects for the E-type asteroid 64 Angelina. *Icarus, 178,* 222–234.

Rousselot P., Petit J.-M., Poulet F., Lacerda P., and Ortiz J. (2003) Photometry of the Kuiper-Belt object 1999 TD_{10} at different phase angles. *Astron. Astrophys., 407,* 1139–1147.

Rousselot P., Petit J.-M., Poulet F., and Sergeev A. (2005a) Photometric study of Centaur (60558) 2000 EC_{98} and trans-neptunian object (55637) 2002 UX_{25} at different phase angles. *Icarus, 176,* 478–491.

Rousselot P., Levasseur-Regourd A. C., Muinonen K., and Petit J.-M. (2005b) Polarimetric and photometric phase effects observed on transneptunian object (29981) 1999 TD_{10}. *Earth Moon Planets, 97,* 353–364.

Rousselot P., Belskaya I. N., and Petit J.-M. (2006) Do the phase curves of KBOs present any correlation with their physical and orbital parameters? *Bull. Am. Astron. Soc., 38(3),* 565.

Schaefer B. E. and Rabinowitz D. L. (2002) Photometric light curve for the Kuiper belt object 2000 EB_{173} on 78 nights. *Icarus, 160,* 52–58.

Sheppard S. S. and Jewitt D. C. (2002) Time-resolved photometry of Kuiper belt objects: Rotations, shapes, and phase functions. *Astron. J., 124,* 1757–1775.

Shkuratov Yu. G. (1987) Negative polarization of sunlight scattered from celestial bodies: Interpretation of the wavelength dependence. *Sov. Astron. Lett., 13,* 182–183.

Shkuratov Yu. and Ovcharenko A. (2002) Experimental modeling of opposition effect and negative polarization of regolith-like surfaces. In *Optics of Cosmic Dust* (G. Videen and M. Kocifaj, eds.), pp. 225–238. NATO Sci Series, Kluwer, London.

Shkuratov Yu., Ovcharenko A., Zubko E., Miloslavskaya O., Nelson R., Smythe W., Muinonen K., Piironen J., Rosenbush V., and Helfenstein P. (2002) The opposition effect and negative polarization of structurally simulated planetary regoliths. *Icarus, 159,* 396–416.

Shkuratov Yu., Videen G., Kreslavsky M. A., Belskaya I. N., Ovcharenko A., Kaydash V. G., Omelchenko V. V., Opanasenko N., and Zubko E. (2004) Scattering properties of planetary regoliths near opposition. In *Photopolarimetry in Remote Sensing* (G. Videen et al., eds.), pp. 191–208. NATO Sci Series, Kluwer, London.

Shkuratov Yu. G., Stankevich D. G., Petrov D. V., Pinet P. C., Cord Au. M., and Daydou Y. H. (2005) Interpreting photometry of regolith-like surfaces with different topographies: Shadowing and multiple scatter. *Icarus, 173,* 3–15.

Shkuratov Yu., Bondarenko S., Ovcharenko A., Videen G., Pieters C., Hiroi T., Volten H., Hovenier J., and Munos O. (2006) Comparative studies of the reflectance and degree of linear polarization of particulate surfaces and independently scattering particles. *J. Quant. Spectrosc. Radiat. Transfer*, *100,* 340–358.

Tholen D. J. and Tedesco E. F. (1994) Pluto's lightcurve: Results from four oppositions. *Icarus, 108,* 200–208.

Verbiscer A. J., French R. G., and Helfenstein P. (2005) Saturn's inner satellites at true opposition: Observations during a central transit of the Earth across the solar disk. *Bull. Am. Astron. Soc., 37,* 702.

Zellner B., Leake M., Lebertre T., Duseaux M., and Dollfus A. (1977) The asteroid albedo scale. I. Laboratory polarimetry of meteorites. *Proc. Lunar Sci. Conf. 8th,* pp. 1091–1110.